Description of fatigue damage in carbon black filled natural rubber

J.-B. Le Cam [a,*], E. Verron [b], B. Huneau [b]

[a] *Laboratoire de Mécanique et Ingénieries - IFMA/UBP, BP 265, 63175 Aubière cedex, France*

[b] *Institut de Recherche en Génie Civil et Mécanique - UMR CNRS 6183, Ecole Centrale de Nantes, BP 92101, 44321 Nantes cedex 3, France*

Abstract

The present paper deals with fatigue damage at the macroscopic scale in carbon black filled natural rubber under uniaxial loading conditions. Uniaxial tension-compression, fully relaxing uniaxial tension and non-relaxing uniaxial tension loading conditions were applied until samples failure. Results, summarized in a Haigh diagram, show that only one type of fatigue damage is observed for uniaxial tension-compression and fully relaxing uniaxial tension loading conditions, and that several different types of fatigue damage take place in non-relaxing uniaxial tension loading conditions. The different damage types observed under non-relaxing uniaxial tension loading conditions are closely related to the improvement of rubber fatigue life. Therefore, as fatigue life improvement is classically supposed to be due to stress-induced crystallization, a similar conclusion can be drawn for the occurrence of different types of fatigue damage.

Key words: rubber, fatigue damage, Haigh diagram, stress-induced crystallization

1 Introduction

Elastomers are extensively used in industrial applications because of their large elastic deformation and great damping capabilities. Elastomeric parts, such as tires, seals, engine mounts, are often subjected to cyclic loading conditions in service. Thus, the study of fatigue characteristics of rubber is of major importance for both design and maintenance of structures.

Research works dealing with fatigue of elastomers have been carried out since the 1940s. Cadwell et al. [1] proposed the first published study in which the surprising response of crystallizable elastomers was highlighted: authors show that natural rubber exhibits an improvement of its fatigue life under non-relaxing uniaxial tension loading conditions, i.e. without complete unloading of the sample during fatigue tests. This result was first presented in a nominal strain vs end-of-life number of cycles diagram.

Since the end of the 1990s, numbers of studies dealing with fatigue of carbon black-filled natural rubber (referred to as CB-NR through the rest of the paper) have been proposed [2,3,4,5]. Similarly to Ref. [1], fatigue tests performed on CB-NR reveal an improvement of the fatigue life under non-relaxing uniaxial tension loading conditions; this improvement is classically attributed to stress-induced crystallization [1,6]. Firstly considered for elastomers fatigue by André et al. [2], the Haigh diagram is revealed as the most appropriate manner to highlight fatigue life improvement, i.e. the influence of minimum strain on fatigue life. Even if it was first defined in terms of Cauchy stress, it is nowadays commonly admitted that fatigue life (end-of-life number of cycles) can be

* Corresponding author.
Email address: lecam@ifma.fr (J.-B. Le Cam).

plotted as a function of numerous other mechanical variables such as stretch or strain, strain energy density, etc. However, most of studies dealing with fatigue life only consider one of these continuum mechanics variables without examining the nature of fatigue damage observed at different locations in the Haigh diagram, i.e. for different cyclic loading conditions.

The present paper is dedicated to the macroscopic description of fatigue damage in CB-NR under various uniaxial loading conditions. Thus, we propose to describe fatigue damage in diabolo CB-NR samples and to study the influence of stress-induced crystallization (referred to as SIC through the rest of the paper) on the end-of-life. Different loading conditions (different mean strain and strain amplitude) will be investigated and results will be presented with the help of the Haigh diagram.

The paper is organized as follow. Section 2 describes experimental details: material, sample geometry, fatigue loading conditions and end-of-life criterion. Then, Section 3 presents the results by distinguishing fatigue damage observed for three types of cyclic loading conditions. Results are summarized in a Haigh diagram in order to relate fatigue damage with loading conditions. Finally, a discussion closes the paper in Section 4.

Table 1

Chemical composition of the natural rubber (phr)

Ingredients	NR	Zinc oxide	Plastificant	Carbon black	Sulphur	Stearic acid	Antioxidant	Accelerators
phr	100	9.85	3	34	3	3	2	4

Table 2

Some basic mechanical properties

Properties	Density (g/cm^3)	Hardness (Shore A)	Failure stress (MPa)	Failure stretch (%)
	1.13	58	22.9	635

2 Description of experiments

2.1 Material and samples

The material considered here is a 34 phr [1] CB-NR. Table 1 summarizes its chemical composition and Table 2 gives some basic mechanical characteristics.

The geometry of the samples is similar to the one proposed by Beatty (see Figure 6 p. 1352 in Ref. [7]); it is axisymmetric and usually referred to as "diabolo" or "dumbbell of revolution" sample. It is shown in Figure 1; relevant terms for the following description of fatigue damage are detailed in this figure. Samples are obtained by injection moulding and rubber is adherized on metallic inserts, the compound is cured during 7 min and the mold temperature is set to 160°C. Moreover, in order to overcome ageing problems, samples are frozen at -18°C 48 h after their moulding and they are thawed out 24h before testing. Such sample is designed to induce an uniaxial deformation mode in its median section under both tensile and compressive loading conditions. Nevertheless, due to its specific geometry, it also induces complex, i.e. multiaxial, deformation modes especially in the neighbourhood of metallic

[1] parts per hundred of rubber (in weight)

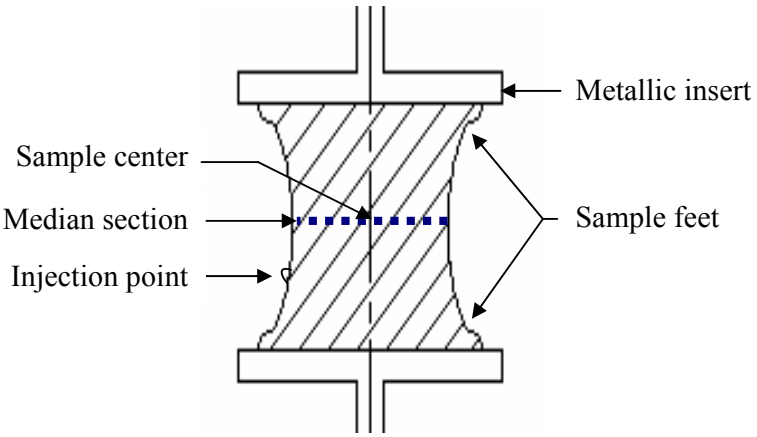

Fig. 1. Diabolo sample.

inserts. In this way, this specimen can be considered as a structure and then may exhibit several types of fatigue damage.

2.2 Fatigue loading conditions

Before detailing fatigue loading conditions, it is first necessary to introduce relevant variables. Experiments are conducted under sinusoidal prescribed displacement. Thus, the uniaxial strain is prescribed under the following form:

$$\varepsilon(t) = \varepsilon_{\text{mean}} + \varepsilon_{\text{ampl}} \sin\left(\frac{2\pi}{f}t\right), \tag{1}$$

where $\varepsilon_{\text{mean}}$ is the mean strain, $\varepsilon_{\text{ampl}}$ is the strain amplitude and f is the loading frequency. Therefore, the minimum and maximum strain during cycles are:

$$\varepsilon_{\min} = \varepsilon_{\text{mean}} - \varepsilon_{\text{ampl}} \text{ and } \varepsilon_{\max} = \varepsilon_{\text{mean}} + \varepsilon_{\text{ampl}}, \tag{2}$$

and the loading strain ratio R_ε is defined by $\varepsilon_{\min}/\varepsilon_{\max}$. In the following, R_ε is simply denoted R. Table 3 summarizes the different values of this ratio in regards to the type of cyclic loading conditions. Here, only three of the seven

Table 3

Different types of cyclic loading conditions

Uniaxial cyclic loading conditions	R
non-relaxing tension	$]0, 1[$
fully relaxing tension	0
tension-compression $\lvert\varepsilon_{\max}\rvert > \lvert\varepsilon_{\min}\rvert$	$]-1, 0[$
symmetric tension-compression	-1
compression-tension $\lvert\varepsilon_{\max}\rvert < \lvert\varepsilon_{\min}\rvert$	$]-\infty, -1[$
fully relaxing compression	$-\infty$
non-relaxing compression	$]1, +\infty[$

possible types of loading conditions were considered in this study: uniaxial tension-compression ($R \in]-1, 0[$), fully relaxing uniaxial tension ($R = 0$) and non-relaxing uniaxial tension ($R \in]0, 1[$) loading conditions. In the following, these loading conditions will simply be described by this corresponding loading strain ratio R. Two parameters chosen into $\varepsilon_{\text{mean}}$, $\varepsilon_{\text{ampl}}$, ε_{min}, ε_{max} and R, and the frequency are needed to completely describe loading conditions; here every loading cases will be defined in terms of ε_{min} and R. Fatigue tests were performed in the Trelleborg french Laboratory in a temperature room regulated at 23°C [4]. The strain rate was set to limit the rise of temperature at the sample surface under 20°C in order to not superimpose thermal damage to mechanical damage; it corresponds to loading frequencies below 5 Hz.

No more details concerning sample dimensions and loading conditions can be given here because of industrial confidentiality.

2.3 Experimental measurement of end-of-life

Two different approaches are classically considered to experimentally determine the end-of-life of samples. Some authors consider that the end-of-life is defined by the number of cycles N_r necessary to break down the sample [1,8]. Others define it by the number of cycles N_i necessary to induce a self-initiated fatigue crack at sample surface [9,10,11a,11b]. In the latter case, the length of the crack is arbitrarily determined: it depends on sample geometry and size, and it is classically related to a significant decrease of sample stiffness. In the present paper, we adopt the second approach by considering the experimental end-of-life measurement recently proposed by Ostoja-Kuczynski et al. [12]: it consists in measuring the sample stiffness and correlating the significant de-

crease of this stiffness with the occurrence of a 2 mm length fatigue crack at sample surface.

Practically, each fatigue test is carried out until sample fracture, both N_r and N_i are recorded.

3 Results

The aim of the present work is to relate the macroscopic fatigue damage to loading conditions, i.e. $\varepsilon_{\min}$ and R. Thus, before presenting our results, it is necessary to precisely define the three different types of cracks that are observed (see Fig. 1 for the description of sample zones):

- large external crack in the median section,
- small external cracks at sample feet,
- cohesive internal crack just below metallic inserts.

In the following, fatigue damage types are presented depending on cyclic loading conditions. Firstly, fatigue damage induced by both $R \in]-\infty, 0[$ and $R = 0$ conditions is described, then fatigue damage induced by $R \in]0, 1[$ condition with two minimum strain levels $\varepsilon^1_{\min}$ and $\varepsilon^2_{\min}$ ($\varepsilon^1_{\min} < \varepsilon^2_{\min}$) is investigated.

3.1 Uniaxial tension-compression ($R \in]-\infty; 0[$) and fully relaxing uniaxial tension ($R = 0$) loading conditions

Only one type of fatigue damage is observed for both $R \in]-\infty; 0[$ and $R = 0$ conditions. It corresponds to initiation and propagation of an external self-initiated crack at the surface of the median section. This crack propagates

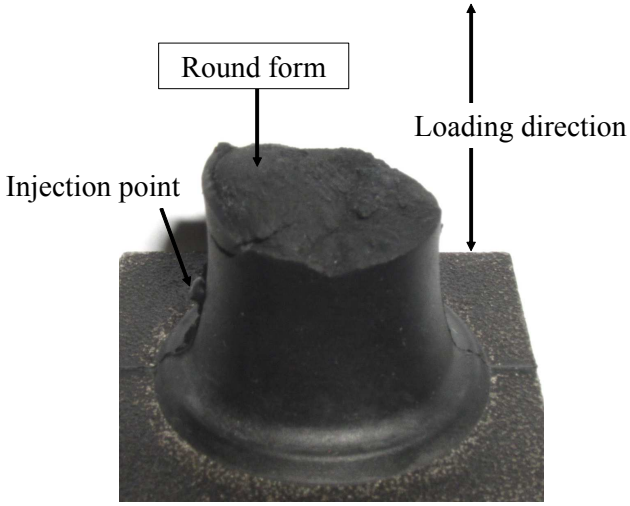

Fig. 2. Fatigue damage type ①

through the median section until sample failure. This is the type of damage that received the most attention in the recent literature [13,14]. Fatigue damage type being identical for both $R \in]-\infty; 0[$ and $R = 0$ conditions indicates that compression loading has no effect on fatigue damage. In the following, it is referred to as damage type ①. Figure 2 presents the fracture surface corresponding to damage type ①. As shown in this figure, a round small surface takes place above the injection point. This zone does not systematically contain the crack initiation zone. This result suggests that cracks propagate circumventing the zone above the injection point. Moreover, the fracture surface is not exactly in the centre of the sample but lightly shifted to the opposite of the injection point. For more information, the reader can refer to Ref. [15]. The influence of the injection point was already observed by Robisson [13] on styrene butadiene rubber.

Even if the median external crack always leads to final rupture for both $R \in]-\infty, 0[$ and $R = 0$ conditions, cutting broken samples reveals small cohesive internal cracks below metallic inserts for high maximum deformation levels

($\varepsilon_{\max} > 200$ %) and $R = 0$ condition. This type of fatigue damage which involves both a median external crack and small internal cracks below metallic inserts will be detailed in Section 3.2.1.

3.2 Non-relaxing uniaxial tension loading conditions $R \in]0, 1[$

Fatigue tests performed with $R \in]0; 1[$ classically exhibit fatigue life improvement in elastomers which crystallize under strain. Thus, as these loading conditions have received less attention than the previous one, this case should be thoroughly examined because we are convinced that the determination of the corresponding damage types will give some relevant informations for the understanding of fatigue life improvement.

In fact, results obtained for $R \in]0; 1[$ will reveal several different damage types. Therefore, in order to simplify the discussion, two minimum strain levels $\varepsilon^1_{\min}$ and $\varepsilon^2_{\min}$ ($\varepsilon^1_{\min} < \varepsilon^2_{\min}$) are distinguished. Because of confidentiality, their values are not given.

3.2.1 Minimum strain level ε^1_{min}

Two fatigue damage types are observed depending on the value of the maximum strain level, i.e. also on R.

- For maximum strain lower than 150%, i.e. $R \in [0.20; 0.33]$, failure of samples is only due to internal cracking below the metallic insert located side of the injection point. However, cutting performed in the neighbourhood of the other metallic insert also revealed internal cracks, but smaller and fewer than in the neighbourhood of the other insert. Figure 3 shows some of these

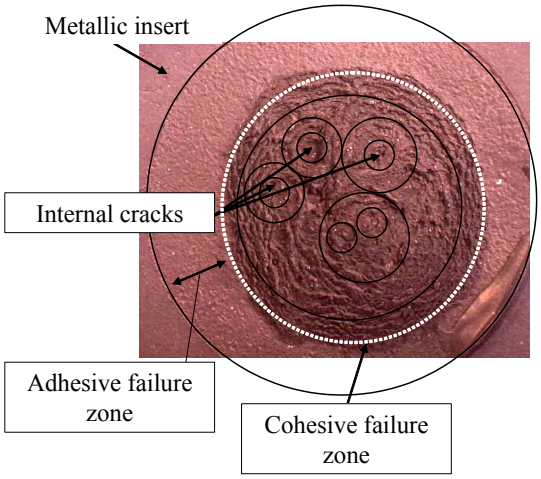

Fig. 3. Nucleation, growth and coalescence of cavities in the bulk material below the metallic inserts. The single circular propagation front cause the final adhesive rupture for $R_\varepsilon \in [0.2; 0.33]$.

internal cracks which propagate, then coalesce and finally produce a single circular front.

This front propagates until sample failure. Failure is first cohesive then it becomes adhesive: the interface between elastomer and the metallic insert is broken down. Furthermore, we performed numerical simulations for static loading of a Diabolo sample which demonstrate that the areas located under metallic inserts are subjected to high hydrostatic pressure conditions. Thus, internal cracks initiate due to high hydrostatic pressure; such cracking phenomenon was previously observed with "Pancake" samples [16,17].

Moreover, another crack is observed closed to the centre of the sample. This crack initiates at sample surface and propagates perpendicularly to the direction of loading (similarly to damage type ①).

This type of fatigue damage, defined by both internal cracks below metallic inserts and one external crack in the center of the sample is referred to as damage type ② in the following.

- For maximum strain greater than 150%, i.e. $R \in [0.14; 0.17]$, samples fail due to the propagation of an external crack in the median section. The corresponding fracture surface is located near sample centre above the metallic insert located on the side of the injection point. Moreover, cutting in the vicinity of metallic inserts reveals internal cracks. This damage type is similar to the one observed for both tension-compression and relaxing tension loading conditions (see Section 3.1) and is already referred to as damage type ③.

3.2.2 Minimum strain level ε^2_{min}

The previous results demonstrate that a competition is established between internal and external cracking for $R_\varepsilon \in]0; 1[$. Thus a question arises: is this competition due to only the maximum strain level or to the whole loading conditions, i.e. defined by two variables for example the minimum and the maximum strain levels ? In fact, this question closely relates to the influence of strain-induced crystallization on fatigue life and of its accumulation under cyclic loading [**?**]. To answer this question, new non-relaxing uniaxial tension loading condition experiments were performed considering a higher minimum strain level $\varepsilon^2_{\min}$ than the former one $\varepsilon^1_{\min}$.

Similarly to previous results under non-relaxing uniaxial tension loading condition, external cracks appear at sample surface and internal cracks develop below metallic inserts. Nevertheless, contrary to previous results, branching occurs, i.e. external cracks do not propagate in the median section of the sample but successively bifurcate in the bulk material. In the following, these cracks [18,19] are called branching cracks.

According to the loading strain ratio R, four different damage types are observed. Let us denote R^i $(i = 1, 4)$ $(R^1 > R^2 > R^3 > R^4)$ the four values of the loading strain ratio and $\varepsilon^i_{\max}$ $(i = 1, 4)$ $(\varepsilon^1_{\max} < \varepsilon^2_{\max} < \varepsilon^3_{\max} < \varepsilon^4_{\max})$ the corresponding maximum strain levels.

(i) $R^1 = 0.36$

Fatigue tests were stopped beyond one million of cycles. As shown in Figure 4, numerous small external cracks are observed on sample surface in the vicinity of sample feet. They are more numerous on the opposite side of the injection point. Surprisingly, these small cracks do propagate neither in bulk material nor on the surface; consequently, they do not lead to sample failure. Finally, cutting samples closed to metallic inserts reveals internal cracks, more numerous on the side of the injection point. The corresponding fatigue damage type is referred to as damage type ④.

(ii) $R^2 = 0.33$

Small external cracks similar to the ones described previously are observed. Moreover, a quasi-vertical branching crack initiates in the bulk material near the metallic insert and propagates on the side opposite to the injection point. Figure 5(a) schematically describes this phenomenon and Figure 5(b) is the top view of the encircled zone in Fig. 5(a).

Cutting the hanging part of the sample (denoted A in Fig. 5(b)) reveals a ring of numerous internal cracks which can be considered as the cause of initiation of the macroscopic crack. This type of fatigue damage is denoted damage type ⑤.

(iii) $R^3 = 0.29$

These loading conditions generate internal cracks closed to the metallic insert on the injection point side. Only three samples were tested: two of them

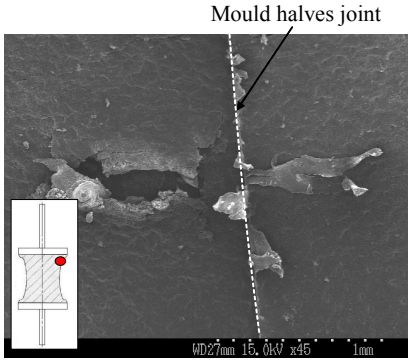

Fig. 4. Small crack at the sample feet obtained under non-relaxing uniaxial tension loading condition (maximum strain level $\varepsilon^1_{\max}$, $\mathrm{R}^1_\varepsilon = 0.36$).

revealed an external crack in sample centre (see Figure 6), this crack propagates by branching. Moreover, cutting revealed internal cracks below the metallic insert opposite to the injection point. This type of fatigue damage is referred to as damage type ⑥.

(iv) $R^4 = 0.25$

These last loading conditions exhibit the competition between external and internal cracking. Indeed, for every tested samples, both internal cracks closed to metallic inserts and an external branching crack in sample centre take place and sample failure is due to one or the other. If failure is obtained by internal crack, damage type is already denoted damage type ⑥, else failure is due to external branching crack and this type of fatigue damage is called damage type ⑦.

4 Discussion

It has been demonstrated that uniaxial fatigue tests performed using diabolo samples lead to seven types of fatigue damage at the macroscopic scale. These

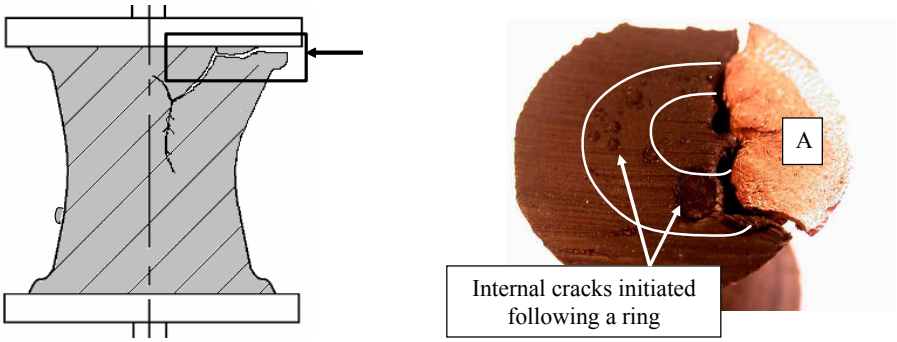

(a) *Schematic view.* (b) *Top view of encircled zone in figure 5(a).*

Fig. 5. Fatigue damage type ⑤ (non-relaxing uniaxial tension loading condition, maximum strain level ε^2_{max}, $R^2 = 0.33$).

Fig. 6. Branching in the centre of the sample (non-relaxing uniaxial tension loading condition, maximum strain level $\varepsilon^3_{\max}$, $R^3 = 0.29$).

types combine internal and external cracks in three zones of the samples. The results are summarized in Table 4.

In order to relate the damage types to loading conditions, we propose to draw a Haigh-like diagram. As fatigue test were performed under prescribed displacement conditions, abscissa represents the mean strain $\varepsilon_{\text{mean}}$ and ordinate represents strain amplitude $\varepsilon_{\text{ampl}}$ (to ensure confidentiality of results, axis are drawn without values); for each loading condition $(\varepsilon_{\text{mean}}, \varepsilon_{\text{ampl}})$, the corresponding fatigue damage type is plotted in Figure 7. Examining this "damage cartography" exhibits that only one type of fatigue damage is observed for both $R \in]-\infty, 0[$ and $R = 0$ conditions and that several different types of fatigue damage take place for $R \in]0; 1[$ conditions. Damage types are schematically presented in Fig. 7 and summarized in Table 4. The unique type of fatigue damage observed for both $R \in]-\infty, 0[$ and $R = 0$ conditions permits to conclude that compression has no effect on fatigue damage. Obviously, the fact that different types of fatigue damage are observed for $R \in]0; 1[$ condition is closely related to the improvement of rubber fatigue life. Therefore, as fatigue life improvement is classically considered to be due to stress-induced crystallization [1,6], a similar conclusion can be drawn for the occurrence of different types of fatigue damage. Furthermore, as crack branching only occurs for $R \in]0; 1[$ condition, the presence of crystallites in rubber can be seen as the cause of fatigue crack bifurcation: in this case, the median section of the sample does not represent the least energetic path for crack propagation.

More generally, results summarized in the previous Haigh diagram should be considered to develop and validate fatigue crack initiation predictors. Indeed, a recent study proposed by Verron et al. [20] demonstrated that only their predictor (the smallest eigenvalue of the configurational stress tensor) is able

Table 4

Summary of the seven types of fatigue damage at the macroscopic scale

Fatigue damage type	large external crack at the surface median section	small external cracks at sample feet	cohesive internal cracks just below metallic inserts
①	yes, propagates to sample failure	no	no
②	yes	no	yes, propagate to sample failure by decohesion between metallic insert and elastomer
③	yes, propagates to sample failure	no	yes
④*	yes	yes	yes
⑤	yes	yes	yes, propagate by branching until sample failure
⑥*	yes, propagates by branching until sample failure	no	yes
⑦	yes, propagates by branching	no	yes, propagate to sample failure by decohesion between metallic insert and elastomer

* fatigue tests stopped before failure

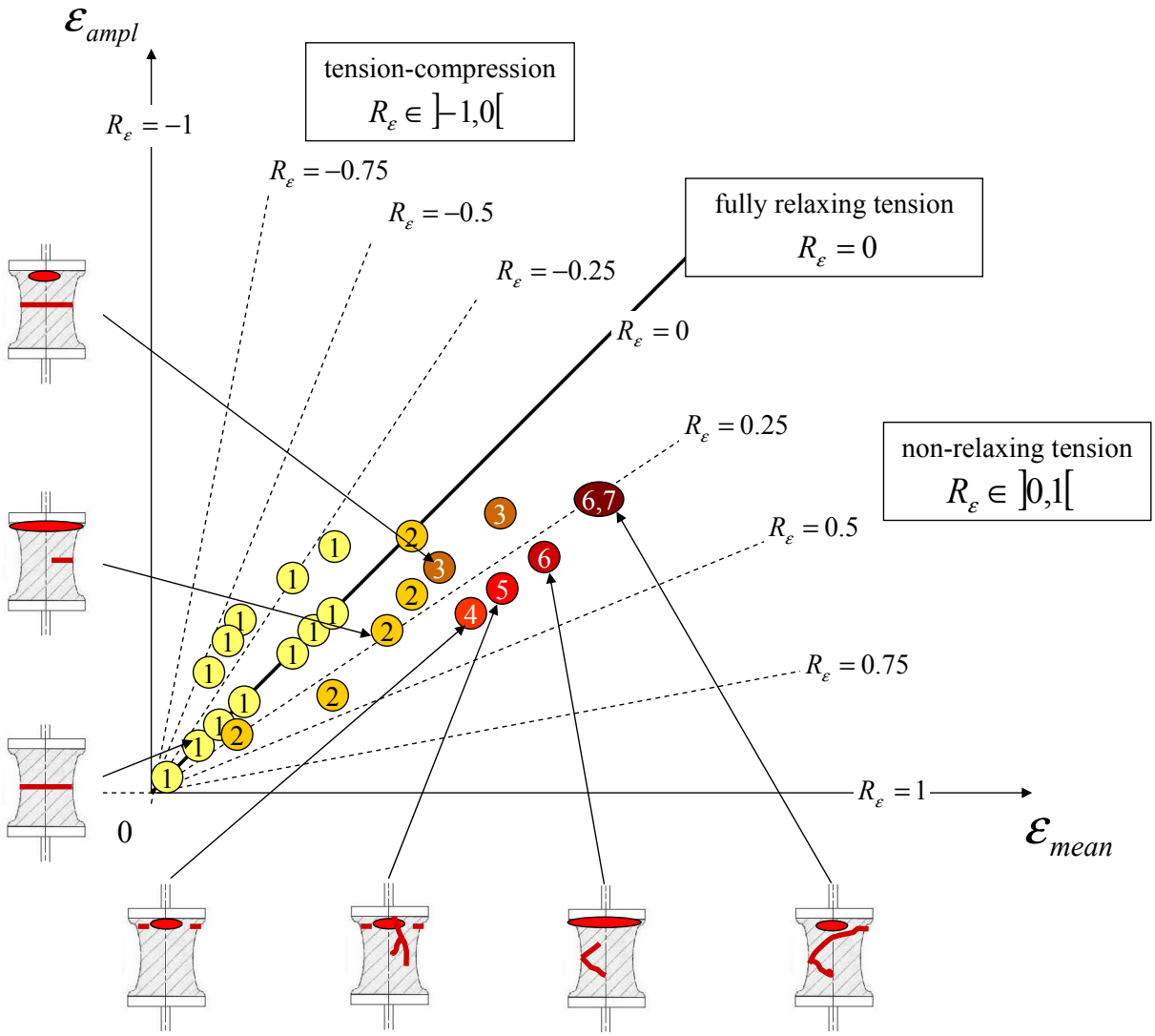

Fig. 7. Haigh diagram of uniaxial fatigue damage observed under prescribed displacement conditions.

to predict the three damage zones of the diabolo sample under uniaxial cyclic loading conditions. An extension of this theory to fatigue life improvement is proposed in Ref. [22].

5 Acknowledgements

Authors would like to acknowledge Allevard Rejna Autosuspensions for its financial support and the Trelleborg french Laboratory for having performed fatigue tests.

References

[1] Cadwell SM, Merril RA, Sloman CM, Yost FL. Dynamic fatigue life of rubber. Rubber Chem Tech 1940; 13: 304-315.

[2] André N, Cailletaud G, Piques R. Dynamic fatigue life of rubber. Haigh diagram for fatigue crack initiation prediction of natural rubber components. Kautsch Gummi Kunstst 1999; 52: 120-123.

[3] Abraham F, Alshuth T, Jerrams S. The dependance of mean stress and stress amplitude of the fatigue life of elastomers. Proceedings of IRC 2001, Birminghan, UK.

[4] Ostoja-Kuczynski E. Comportement en fatigue des élastomères : application aux structures antivibratoires pour l'automobile. PhD Dissertation. Ecole Centrale de Nantes; 2005.

[5] Saintier N, Cailletaud G, Piques R. Crack initiation and propagation under multiaxial fatigue in a natural rubber. Int J Fatigue 2006; 28: 61-72.

[6] Lindley PB. Relation between hysteresis and the dynamic crack growth resistance of natural rubber. Int J Fract 1973; 9: 449-461.

[7] Beatty JR. Fatigue of rubber. Rubber Chem Technol 1964;37:1341-1364.

[8] Roberts BJ, Benzies JB. The relationship between uniaxial and equibiaxial fatigue in gum and carbon black filled vulcanizates. Proceedings of Rubbercon 77, vol. 2.1; 1982. p. 113.

[9] Lu C. Etude du comportement mécanique et des mécanismes d'endommagement des élastomères en fatigue et en fissuration par fatigue. PhD Dissertation, Conservatoire National des Arts et Métiers; 1991.

[10] Xie J. Etude de la fatigue et de la rupture des assemblages collés composite-élastomère. PhD Dissertation, Ecole Centrale de Paris; 1992.

[11a] Mars WV. Multiaxial fatigue of rubber. PhD Dissertation, University of Toledo; 2001.

[11b] Mars WV, Fatemi A. A literature survey on fatigue analysis approaches for rubber. Int J Fatigue 2002; 24: 949-961.

[12] Ostoja-Kuczynski E, Charrier P, Verron E, Markmann G, Gornet L, Chagnon G. In: Muhr A, Busfield J, editors. Constitutive models for rubber III. A.A. Balkema Publishers; 2003.

[13] Robisson A. Comportement mécanique dun élastomère chargé en silice. Etude de linfluence des charges et modélisation par une loi visco-hyperélastique endommageable. PhD Dissertation, Ecole des Mines de Paris; 2000.

[14] Wang B, Lu H, Kim G. A damage model for the fatigue life of elastomeric materials. Mech Mater 2002; 34: 475-483.

[15] Le Cam JB. Endommagement en fatigue des élastomères. PhD Dissertation, Ecole Centrale de Nantes; 2005.

[16] Gent AN. Cavitation in rubber: a cautionary tale. Rubber Chem Technol 1990; 63: G49-G53.

[17] Legorju-Jago K, Bathias C. Fatigue initiation and propagation in natural and synthetic rubbers. Int. J. Fatigue 2002; 24: 85-92.

[18] Kim HJ Hamed GR. On the reason that passenger tire sidewalls are based on blends of natural rubber and cis-polybutadiene. Rubber Chem Technol 2000; 73: 743-752.

[19] Shaw C, Kerchman V. Experimental study and finite element simulation of heat build-up in rubber compounds with application to fracture. Rubber Chem Technol 2003;76:386-405.

[20] Verron E, Le Cam JB, Gornet J. A multiaxial criterion for crack nucleation in rubber. Mech Res Commun 2006; 33: 493-498.

[21] Verron E. Prediction of fatigue crack initiation in rubber with the help of configurational mechanics. In: Austrell PE, Kari L, editors. Constitutive models for rubber IV.Netherlands: Swets and Zeitlinger; 2005.

[22] Andriyana A, Verron E. Prediction of fatigue life improvement in natural rubber using configurational stress. Int J Solids Struct 2007; 44: 2079-2092.